Received: 29 October 2021 | Revised: 27 June 2022 | Accepted: 1 August 2022

DOI: 10.1002/mmce.23363

ORIGINAL ARTICLE

INTERNATIONAL JOURNAL OF RF AND MICROWAVE COMPUTER-AIDED ENGINEERING WILEY

Robust numerical approximation of 2.5-dimensional electromagnetic problems by using finite elements

José Mª. Gil

Departamento de Señales, Sistemas y Radiocomunicaciones, Universidad Politécnica de Madrid, Madrid, Spain

Correspondence
José Mª. Gil, Departamento de Señales, Sistemas y Radiocomunicaciones, Universidad Politécnica de Madrid, Madrid, Spain.
Email: jmg@etc.upm.es

Funding information
This work was partially supported by Ministerio de Ciencia e Innovación (MCIN/AEI /10.13039/501100011033 / FEDER, UE) under project PID2021-122856NB-C22

Abstract

When a numerical method is used to analyze or design an electromagnetic structure, as the finite element method, the introduction of the behavior of some component of the electromagnetic field (when this is known) allows to project the physical problem onto a two-dimensional mesh, multiplying the capacity of the method to make efficient computer aided design of complex devices as they are demanded nowadays. Though this is an old issue, which has been focused one or two decades ago, the arrival of higher-order function basis and powerful tools of meshing and post processing makes interesting to review this important field within the computational electromagnetic area.

KEYWORDS

BOR structures, conical horns, high-order finite elements, spurious solutions

1 | INTRODUCTION

The 3D finite elements method (FEM) is an extensively accepted tool for analysis and design of microwaves/millimeter circuits and antennas based on the use of complex materials and geometries. Despite the huge memory capacity and computation speed of the current informatics systems, the method still suffers from an expensive computational cost when the domain is 3D. In many practical structures, the knowledge of the behavior of some field component or the presence of some symmetry allows the discretization of the Maxwell equations onto a bi-dimensional mesh, reducing dramatically the computational cost of the analysis. That is the case of homogeneous waveguides, where we only need to discretize two or even one field component or scalar potential (TEM/TE/TM modes), and then obtain the rest of components by means of post processing approaches. When the structure is no homogeneous, it supports hybrid modes and the three components of the electromagnetic vector field must be approximated in the formulation and they must be projected onto a three dimensional mesh. Many of these practical problems can take advantage of some symmetries as the knowledge of the variation of one of its field components along a coordinate. They make up many and much known structures, as they are transmission lines and waveguides with translation symmetry, E-Plane and H-Plane unions, dielectric resonators (DR) based on bodies of revolution (BOR) and antennas with rotational symmetry like conical horns, monopoles, dielectric antennas or lens. They have been called 2.5 dimensional problems by the finite elements community due to the need to approximate the three components of the field, but the mesh of the discretized problem has a bi-dimensional (2D) character. This type of problems have been intensively studied by many researchers along

the last two decades.[1–8] These approaches provide a huge potential to configure computer aided design (CAD) tools in conjunction with the last developments relative to pre and post processors, new and more powerful meshers and solvers, and the need of adding new higher-order basis functions to the formulations. It may worth to review these procedures, trying to increase its reliability and robustness. It should be a priority to incorporate the use of higher-order elements to the discretization of these 2.5-dimensional problems, facing complex geometries by containing field singularities, diverse materials and multiscale details with curved boundaries. They conform the structures that electrical engineers handle nowadays. This work is an extension with some new results of previous one presented at.[9] We show some results about the analysis of an anisotropic dielectric resonator that, in conjunction with those at,[6] recommend the use of basis functions of orders greater than two may. The relation between the different subspaces that conform the overall function vector space is studied to avoid the apparition of the undesirable spurious solutions for any order of the basis. Moreover, we use a mixed 2.5-dimensional finite elements-modal analysis approach, described in[5] to design a profiled conical dielectric-core horn antenna ended by dielectric lens, showing an optimal performance of this tool for the computer assisted design of such complex antennas.

Some conical diel-core horns, ended by lens, have been studied following different approaches to the proposed in this work and they can be found in recent literature.[10,11]

2 | HYBRID FINITE ELEMENTS FOR 2.5-DIMENSIONAL PROBLEMS

A family of higher-order basis functions conforms a kind of hybrid finite element in which the transverse (meridian) component of the field (electric or magnetic) is approximated by a vector space maintaining its vector character, that is, it is not decomposed into its two components. The family of Lagrange polynomials of any order is reserved to span the axial (azimuthal) component of the field. We focus on two kinds of problems presenting two symmetries. One of them is relative to structures having translation symmetry in which the electric/magnetic field (Ψ) is separated into two components, one is transverse and vectorial and the other is axial and scalar; they correspond to modes in transmission lines and waveguides, that is being β, the propagation constant of the mode.

$$\vec{\Psi}(x,y,z) = \left[\vec{\Psi}_t(x,y) + \Psi_Z(x,y)\hat{z}\right]e^{-i\beta z} \tag{1}$$

The other type of problems has rotational symmetry. The meridian component of the fields is a vector and the azimuthal component is a scalar; they are problems based on BOR's.

$$\vec{\Psi}(r,\varphi,z) = \left[\vec{\Psi}_t(r,z) + \Psi_\varphi(r,z)\hat{\varphi}\right]e^{-i\beta\varphi} \tag{2}$$

$$\Psi = \mathrm{E}\,\mathrm{or}\,\mathrm{H}$$

β, is the azimuthal order of the mode.

2.1 | Basis functions for both transverse and axial (azimuthal) components

In order to set up the ideas, we focus on a multi-material section with a rotational symmetry by conforming a BOR. If Γ is the boundary of the structure in the meridian plane and is a perfect electrical/magnetic wall, then we have a multi-dielectric resonator inside a cavity enclosure. It also is called an axisymmetric structure (Figure 1).

The electromagnetic fields are expanded as a series of axisymmetric modes expressed as

$$\vec{\Psi} = \sum_{m=0}^{m=\infty}\left[\vec{\Psi}_t(r,z)sinm\varphi + \frac{1}{r}\Psi_\varphi(r,z)cosm\varphi\hat{\varphi}\right] \tag{3}$$

They are divided into φ-independent modes ($m = 0$), called $\mathrm{TE_{0ld}}$ and $\mathrm{TM_{0ld}}$, and hybrid modes with a known φ-dependence ($m \geq 0$), called $\mathrm{HE_{mld}}$. We span the two components of the field, transverse or meridian (r, z), and azimuthal (φ) separately. We use a set of higher-order vector hierarchical basis functions for the transverse component, configuring a vector tangential finite element for this component, and a scalar nodal element for the azimuthal component. This is a 2.5-dimensional hybrid element and we add the corresponding high-order coordinate transformation in order to deal with curve domains. Some similar approaches are found in literature although they use only lowest-order elements, being not reliable enough to the very complex geometries that are demanded nowadays.[3] The fields in (3) are spanned as follows; the transverse component

$$\vec{\Psi}_t(r,z) = \sum_{i=1}^{N_t}\Psi_{ti}\vec{\mathrm{T}}_i(r,z) \tag{4}$$

N_t is the number of transverse functions for the meridian component, and T_i are curl-conforming basis functions. The azimuthal component is

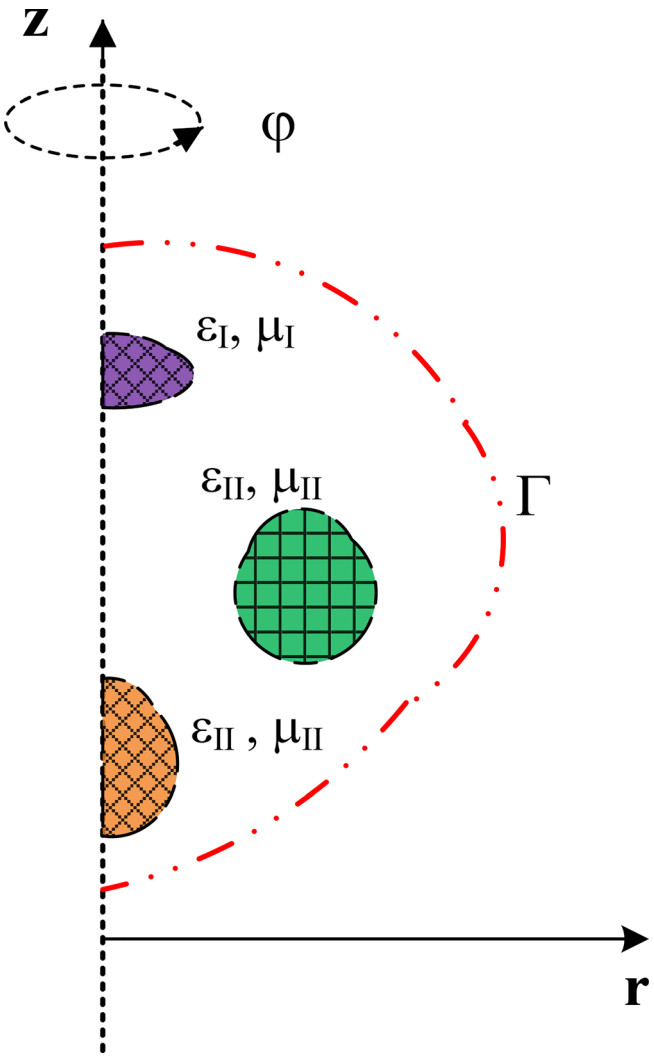

FIGURE 1 Axisymmetric Structure.

$$\Psi_{\varphi}(r,z)=\sum_{i=1}^{N_{\varphi}}\Psi_{\varphi i}L_i(r,z) \tag{5}$$

N_{φ} is the number of azimuthal functions for the φ component and L_i are the Lagrange polynomials of any order.

2.2 | Decomposition into subspaces

The vector space of functions for the overall problem 2.5-dimensional is

$$\underset{mnq}{\tilde{V}}=\left(G_m\bigoplus R_n\bigoplus S_q\hat{\zeta}\right)e^{-i\beta\zeta} \tag{6}$$

being $\hat{\zeta}=\left\{\hat{z}\,or\,\frac{\hat{\varphi}}{r}\right\}$, depending on the symmetry of the structure. The $\underset{mnq}{V}$ space is decomposed into three subspaces. G_{m} is the subspace of transverse irrotational (curl-free) basis functions, or static subspace, its order is m. R_{n} is the subspace of transverse rotational (curl) basis functions, its order is n. S_{q} is a subspace of 2D Lagrange polynomials of q degree. Moreover, we can denote

$$V_{mn}=G_m\bigoplus R_n \tag{7}$$

V_{mn}, is the transverse vector space of functions that spans the transverse or meridian component of the field. This space is decomposed into an irrotational subspace of transverse functions and a transverse rotational subspace; that is known as Helmholtz decomposition,

$$G_m=\left\{\vec{g}\,\epsilon\,V_{mn}/\nabla_t\times\vec{g}=0\right\} \tag{8}$$

$$R_n=\left\{\vec{r}\,\epsilon\,V_{mn}/\nabla_t\times\vec{r}\neq 0\right\} \tag{9}$$

Therefore, if G_m is the static subspace, the vectors $\vec{g}$ are gradients of scalar functions, $\vec{g}=\nabla_t V$, and $G_m=\nabla_t S_{m+1}$. If the static subspace is of order m and it is used with a rotational subspace or order m or m + 1, spurious solutions does not appear; that is true for a 2D, or even a 3D problem. Nevertheless, may it be extrapolated to the 2.5-dimensional case? Then, how is the static subspace of the whole problem? This subspace is formed by irrotational or curl-free $\vec{\Psi}$ functions. Then

$$\nabla\times\vec{\Psi}=0 \tag{10}$$

The $\vec{\Psi}$ function has two components, one is a vector transversal and the other is a scalar azimuthal (or axial), as we have seen

$$\vec{\Psi}=\vec{\Psi}_t+\Psi_{\zeta}\hat{\zeta} \tag{11}$$

The condition (10) occurs when the two following expressions are given at same time

$$\nabla_t\Psi_{\zeta}+j\beta\vec{\Psi}_t=0 \tag{12}$$

$$\nabla_t\times\vec{\Psi}_t=0 \tag{13}$$

From (13), we yield that the transverse component is the gradient of a scalar function V, that is, $\vec{\Psi}_t=\nabla_t V$.

And substituting in (12) we obtain

$$\Psi_\zeta = -j\beta V + K \tag{14}$$

We conclude that the irrotational functions of the static space are of the form

$$\nabla_t V - j\beta V\hat{\zeta} \tag{15}$$

for some scalar function, V. That means the static functions have a component in the static transverse subspace G_m and another component in the azimuthal (axial) subspace S_q. If $\beta = 0$, the irrotational or "static" subspace of the space of discrete functions is just the space of transverse gradients. When this space is of order m, and used with a transverse rotational space R_n of order $n = m$ or $n = m + 1$, spurious solutions do not occur; the discrete irrotational subspace is big enough to approximate properly the static eigenmodes ($k = 0$) that might otherwise be poorly approximated and show up as spurious modes in the computed spectrum.[12]

If $\beta \neq 0$, the static subspace is no longer identical to the space of transverse gradients. However, it has been shown that every static function is of the form of (15). If the space of axial functions is of order $m + 1$ (or greater) and the transverse gradient space is of order m, the static subspace will be the same size as the transverse gradient space. Any reduction in the order of the subspace of the azimuthal (axial) functions S_q will reduce the static subspace and may lead to spurious modes. The important conclusion is valid for any order of the vector spaces and it stablishes the order among the three subspaces. These orders can be expressed by means of the triplet (m, n, q), satisfying the following requirement

$$q = m + 1 \tag{16}$$

-These elements can be seen as the composition of two elements conforming a hybrid finite element, a vector transverse finite element with the basis functions associated to the edges and faces, and a nodal scalar element in which the basis functions are associated to the nodes at the vertex and along the edges (Figure 2). They are curved of any order of curvature and they form a hierarchical family, that is, we obtain an element adding degrees of freedom and functions to the element of order immediately lesser. Furthermore, because the transversal elements associate the degrees of freedom with edges and faces instead of vertices, field singularities can be handled with a better accuracy. Earlier works,[4,13] have used lower-order functions, except,[14] where polynomials to order three were used. They have chosen the correct order for the axial/azimuthal component but they have used only a criterion of consistency with the order of the approximation of the transverse component instead to apply one demonstrated criteria as expressed in (16); moreover, they avoid the use of higher-order elements.

In Table 1, we can see the ordination of the elements of increasing order with the dimension of the subspaces in relation to the triplet (m, n, q).

2.3 | Spurious modes after discretizing a dielectric fiber

In Figure 3, the wavenumber for a propagation constant $\beta = 10.9215$ rad/cm, of both the HE11 mode and the first highest mode, for a dielectric fiber of diameter $d = 1$ cm, is shown. The fiber is embedded in air and closed by an artificial PEC boundary located at 1.25 cm from the centre of the fiber. The permittivity of the fiber is $\varepsilon_r = 2.25$.

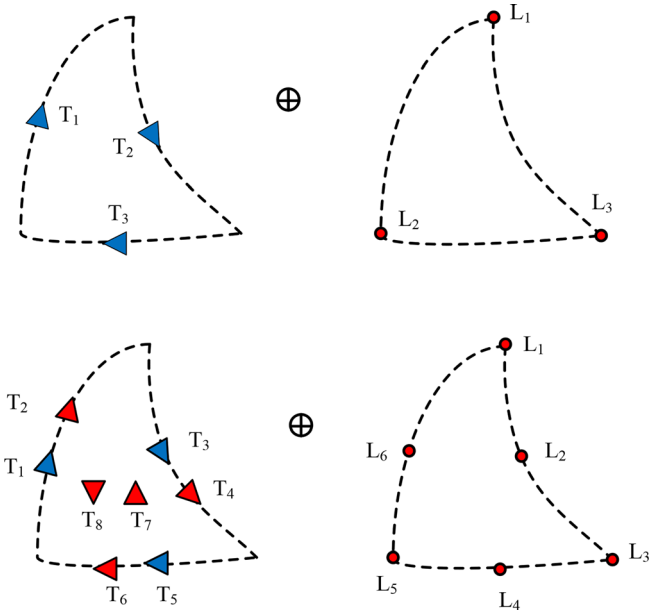

FIGURE 2 Hybrid (0, 1, 1) and (1, 2, 2) elements.

TABLE 1 Subspace orders.

Element (m, n, q)	G_m	R_n	S_q	$\widetilde{V}_{mnq}$
(0, 1, 1)	0	3	3	6
(1, 1, 2)	3	3	6	12
(1, 2, 2)	3	5	6	14
(2, 2, 3)	7	5	10	22
(2, 3, 3)	7	8	10	25
(3, 3, 4)	12	8	15	35
(3, 4, 4)	12	12	15	39
...				

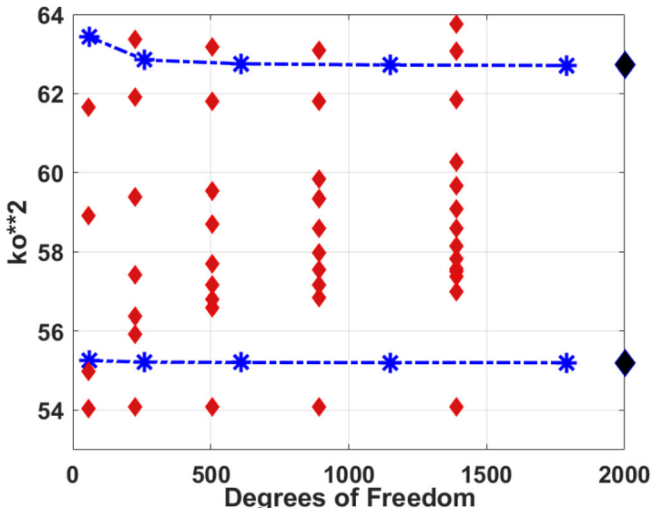

FIGURE 3 Spurious modes (♦) between the first two modes in a fiber solved with (1, 2, 1) elements. □, correct modes computed with elements of order (1, 2, 2).♦, exact values.

TABLE 2 Basis functions of order (1, 2, 2).

Rotational functions (edges)	T_{ip} (p, q)	T_{iq} (p, q)
T_1	1−q	p
T_2	−q	p
T_3	−q	p−1
Gradient functions (edges)		
T_4	1−2p−q	−p
T_5	q	p
T_6	−q	1−p−2q
Rotational functions (face)		
T_7	q (1−2p−q)	p (−2 + q + 2p)
T_8	q (1 + p−q)	p(1−p + q)
Scalar polynomials (Lagrange)		
L_1	(1−p−q)(1−2p−2q)	
L_2	p(2p−1)	
L_3	q(2q−1)	
L_4	4p(1−p−q)	
L_5	4pq	
L_6	4q(1−p−q)	

The wavenumber is computed by using two elements with two different values for the order of the scalar subspace S_q, maintaining the same order of the transverse subspaces; these orders are (1, 2, 2) and (1, 2, 1), respectively. When the (1, 2, 1) element is used, spurious solutions appears in the spectrum and its number increases in relation to the refinement of the mesh. In opposite, a clear spectrum of spurious is obtained when the (1, 2, 2) element is used, supporting the requirement $q = m + 1$.

The T_i tangential vector functions in (4) are expressed in a master element through a coordinate transformation. The real coordinates (r, z) in transverse plane are transformed into local coordinates (p, q) in a reference plane.

$$\vec{T}_i(r,z) = T_{ip}(p,q)\nabla p + T_{iq}(p,q)\nabla q \tag{17}$$

T_{ip}, T_{iq} are the covariant components and ∇p, ∇q are the base reciprocal vectors. For example, the covariant components, together with the scalar polynomials (18) to span the axial (azimuthal component), for an element of order (1, 2, 2), are given in Table 2.

3 | APPLICATIONS TO BOR

3.1 | Dielectric Resonators enclosed in cavities

An interesting application of this type of elements is the computation of resonance frequencies of modes in DR enclosed in metallic cavities. They can be miniaturized and stabilized to be part of microwave integrated circuits (MIC). The geometry is shown in Figure 1. The electromagnetic field variates as (3), and the equation to be discretized is the wave equation that, after applying the Galerkin method is

$$\int_V \left(\nabla \times \vec{H}\right)[\varepsilon_r]^{-1}\left(\nabla \times \vec{H}\right)^* dV - k_o^2 \int_V \vec{H}[\mu_r]\vec{H}^* dV = 0 \tag{18}$$

k_o is the wavenumber of the mode; it is obtained from the eigenvalues of the system of equations which result of the discretization of the physical problem. A dual approach may be formulated if the electric field is used instead of magnetic field in (18).

In Figure 4, a rod sapphire dielectric resonator enclosed in a metallic cavity is shown. This uniaxially anisotropic resonator is hold by a support with a permittivity closed to the air. The sapphire has an anisotropy characterized by a tensor permittivity given by ε_{tt} and ε_z. In Figure 5, we can see the performance of several hybrid higher-order elements in the computation of the resonant frequency of the EH_{11d} mode. The frequency is in GHz. The reference corresponds to results given by.[15] Because we use H-field in this case,

this is not as strong as the E-field in the neighborhood of the edge of the crystal; then, the order of Rotational space is relevant for a reliable approximation of the field. This order is the second number of the triplet (m, n, q). Results suggest do not use orders lower than two.

When higher-order modes must be computed for some application, a higher-order element is then more determinant to obtain a reliable description of the field. That is the case of the called Whispering-gallery modes (WGM) which have important applications for determining the characteristics of materials, or for designing stable microwave oscillators. The WGM are hybrid modes with a high azimuthal variation and then they suffer of a high spectral density being contaminated by the cavity modes perturbed by the dielectric material. Therefore, an accurate computation of resonant frequencies and fields could be determinant to the designer to get DR's working with WGM's in a free-spurious modes window. Resonant frequencies for a few WGM, in the DR shown in Figure 4, have been computed by using (1, 2, 2) elements. They are shown in Table 3. Results are compared with those by.[16]

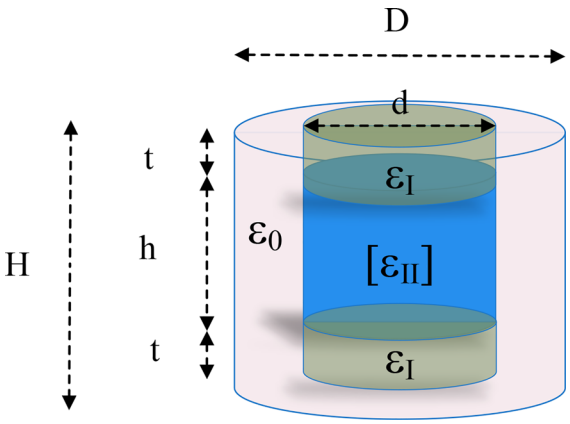

FIGURE 4 Rod sapphire DR. $h = 1$ cm, $H = 1.3$ cm, $d = 1$ cm, $D = 15.6$ cm, $\varepsilon_I = 1.031$, $\varepsilon_{tt} = 9.389$, $\varepsilon_{zz} = 11.478$.

3.2 | Horn antennas based on BOR

An efficient method for the analysis and design of radiating structures based on BOR was developed in the early twenties.[5] The approach was based on a segmentation of the azimuthal plane into some regions and the use of finite elements for the discretization of the wave

TABLE 3 Resonant frequencies for a few wgm's in a sapphire DR.

Mode	f_o (GHz)	[16]
$HE_{11\ 1\ d}$	8.3285	8.3283
$EH_{11\ 1\ d}$	9.7867	9.7871
$HE_{12\ 1\ d}$	8.9493	8.9487
$EH_{12\ 1\ d}$	10.4756	10.4740

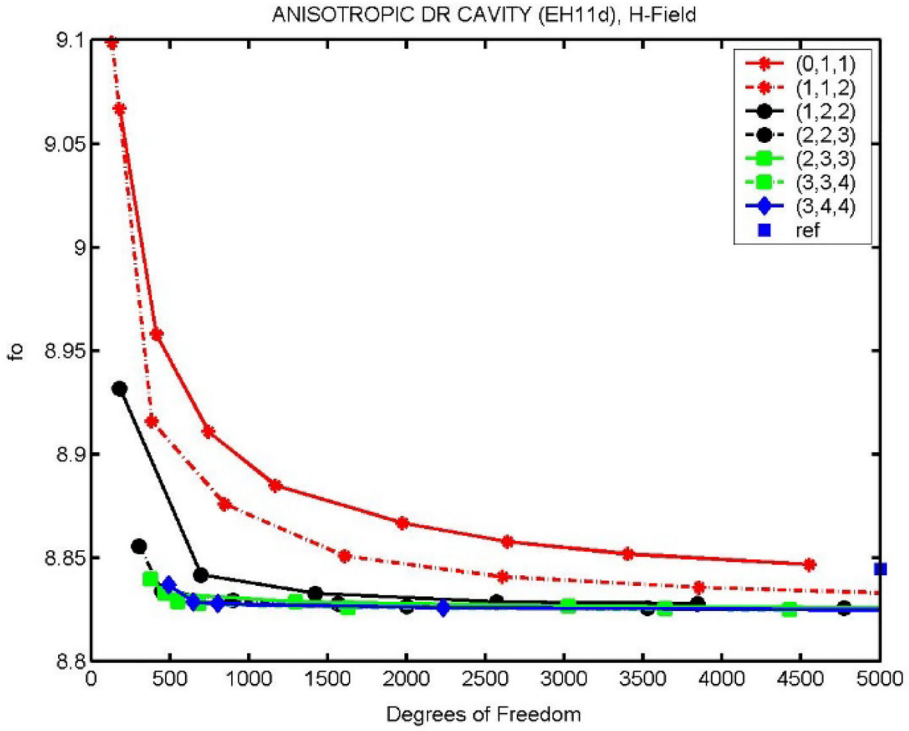

FIGURE 5 Performance of higher-order hybrid elements.

equation. The antenna is characterized as a closed circuit, with a port simulating the input waveguide and a second spherical port closing the radiator and defining a boundary where a spherical mode expansion of the fields is used. The discretization of such kind of problems copes well with the finite 2.5-dimensional elements. The analysis of horn based on BOR has been undertaken by different authors by using others approaches. For example,[17] although the authors use a Perfect Match Layer to close the finite element domain instead of an expansion of spherical modes as in the current method. From the first approaches proposed to the last ones nowadays, some of the employed tools have seen several important advances, improving substantially its performance. Among the formers are the new higher-order hybrid elements, pre and post processors with very powerful meshers, or new solvers, which speed up the computation of the solutions, and the dramatic increasing of the capacity of the computers. These improvements motivate a revision of some known radiating structures as the conical horns loaded with dielectrics and lens. We study some horns based on classical designs and we show some interesting variations that can be added to the original designs. The antennas are studied following the approach described in,[5,18] with optimized basis functions of higher-order.

They are characterized as a multimode, two ports microwave circuit, where the port 1 is a feed port and a spherical surface surrounding the antenna constitutes the port 2 of the circuit, which is then described by its generalized scattering matrix (GSM). (Figure 6).

The spherical surface defines a computational domain for the radiating region. This region may be reduced assuming that the sphere intercepts the conical surface of the horn far enough from the aperture to have negligible fields (and currents) along the interception surface (Figure 6). To find the optimal radio of the spherical port, a previous study of convergence must be done. Furthermore, the size of the mesh is also decided by considering that the numerical convergence has been achieved.

Once the GSM is computed, the [S] parameters establish the relations among the modes in the input waveguide and the spherical modes in the spherical guide; the radiation patterns, return losses, directivity, beam widths or aperture efficiency of the antenna are then easily determined.

3.2.1 | 2a- Dielectric-loaded horn antennas

Conical metallic horns loaded with a dielectric cone achieve perfectly symmetric radiation patterns and low-peak of cross-polarization level on a wide frequency band. These antennas are used as feeds for reflectors as

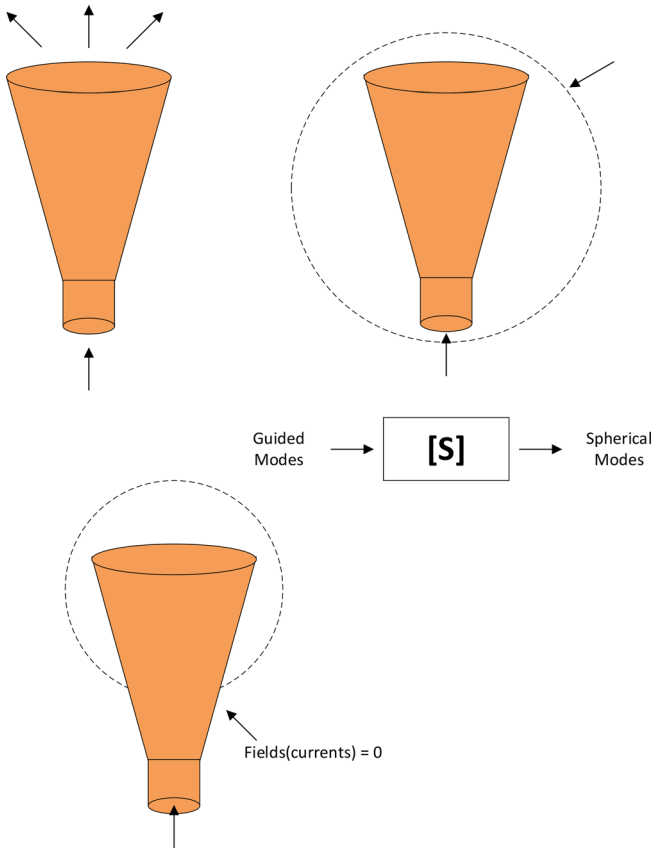

FIGURE 6 Antenna based on BOR characterized as a two ports circuit.

an alternative to corrugated horns, especially at highest frequencies because of its simplicity of manufacture. The addition of a dielectric core in the horn creates hybrid modes (HE11) in the aperture modifying the radiation pattern. A low-peak of cross-polarization is achieved on wide frequency bands.

The current method was applied to the analysis of a classical dielcore horn, as shown in Figure 7.

The geometrical data are the following: $L = 34.3$ cm (11.43 λ); $r = 1.143$ cm; d/2 = 6.5 cm; D/2 = 7.7 cm ($D = 5.13\ \lambda$); $g = 1.2$ cm. The central frequency is $f = 10$ GHz (X-Band). The dielectric core is formed by foam polyestyren ($\varepsilon_r = 1.13$), and the radio of the spherical port is $R = 11.705$ cm. The mesh uses 13 960 elements of order (1, 2, 2), and 28 335 geometrical points, once the h-convergence is achieved. After a study of the modal convergence, we use the first 5 modes in the input circular waveguide and 100 spherical modes in the spherical port. The computation time is short, around some seconds running in a personal computer, demonstrating how powerful may be this tool to optimize this kind of antennas, including the profile of the taper of the horn, or adding lenses to focus the radiation pattern of the antenna, as we will see in the following examples. The obtained results are

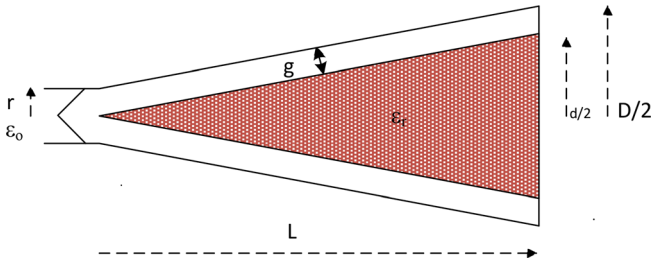

FIGURE 7 Conical horn with a dielectric core.

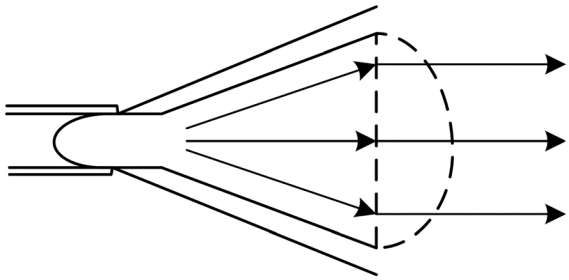

FIGURE 8 Dielectric horn + a convex lens.

TABLE 4 Performance of a dielectric loaded conical horn.

Parameter	This work	[19]
D (d B)	21.8	22.1
EA (%)	58.1	61.8
XP (d B)	−32.3	−32.2
BWcop (°)	15.1	14.8
VSWR	1.08	1.04

Abbreviation: BWcop, beam width in the copolar; EA, efficiency of aperture; XP, peak of the cross-polar.

compared with those by Olver et al.[19] in the Table 4, where D is the directivity, EA is the efficiency of aperture, XP is the peak of the cross-polar diagram and BWcop is the beam width in the copolar pattern.

Additive manufacturing technology has gathered an increasing attention due to the facility to handle arbitrary geometries and internal dielectric materials.[20] The use of 3-D printers provides the dielectric core and, after a metal plating of the outer surface, an inexpensive and fast prototype can be achieved. An outer dielectric to support the core is added by using a foam with a permittivity close to one.

The profiling of the horns leads to some benefits over the linear flare angle horns. The length of the horn can be reduced and due to that, the flare angle at the aperture is almost zero; the phase center is keep near to the aperture, improving the efficiency and the frequency response of the antenna. We can also improve the efficiency and other radiation characteristics by the addition of lenses (Figure 8).

The lens can conform a plane phase pattern at the aperture, achieving the efficiency and the bandwidth of the horn. Moreover, we can design the profile of the lens to improve some radiation parameter as the cross-polarization.

Along the following, we are going to improve a linear dielectric horn like shown in Figure 7, but we use a foam as the outer dielectric with a permittivity of 1.04 at 10 GHz. The permittivity of the core is then optimized obtaining a value of $\varepsilon_r = 1.2$. We optimized the radiation parameters shown in Table 4. The XP and mod (S11) are improved to −36.8 dB and −35.1 dB, respectively. By means of the profile of the horn and the addition of lens, we can improve even more the behavior of the antenna.

The profile of the horns has been optimized by different authors by using global optimization algorithms with a huge charge of computational cost; the profiles obtained by such techniques results to be pseudo-harmonics or pseudo-sinusoidal, giving designs with a not stable behavior in wide frequency ranges.[5,21]

In the next, we propose an improved dielcore horn in which we try to reduce the return losses and the peak cross-polar and to increase the efficiency and the directivity; to achieve it, we profile the taper, optimize the value of the permittivity of the dielectric core and we add a lens in the aperture of the horn. The type of profile relates to the amplitude and phase of the modes at the aperture whereas focuses the radiation, improving the directivity and then, the efficiency; the used profile is polynomial and its equation is as follows

$$r(z) = r + 3\Delta r\left(\frac{z}{L}\right)^2\left(1 - \frac{2z}{3L}\right) \tag{19}$$

$$\Delta r = \frac{D}{2} - \mathrm{r}$$

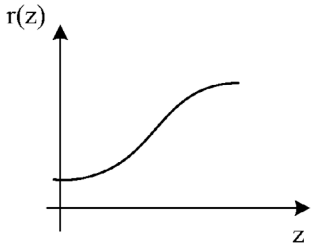

where D is the diameter of the aperture, r is the radio of the throat and L is the length of the horn.

In order to reduce the return losses, a matching section is used at the throat of the horn; the profile of the core at the throat is optimized looking for a minimal reflection. We have noticed differences of 10 dB in the

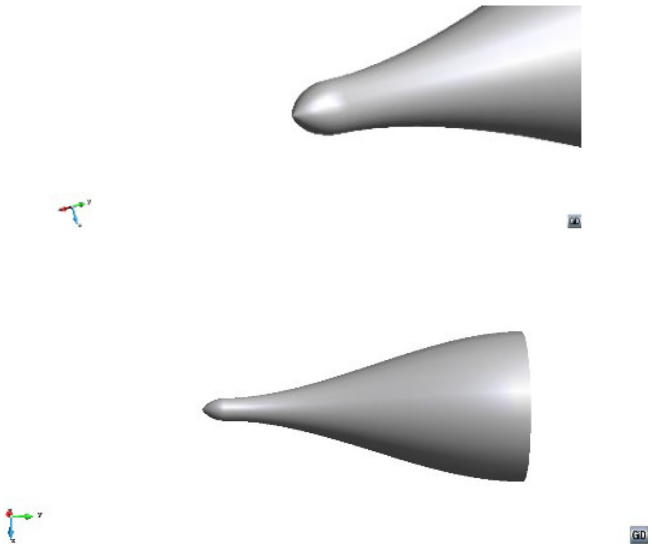

FIGURE 9 Smoothing shape of the throat of the dielectric core.

FIGURE 10 Profiled dielcore horn with a convex lens.

return losses by using several shapes. A smoothing of the sharp tip of the core produces a significant reduction of the return losses (see Figure 9).

The two dielectrics may be manufactured by means of 3D additive techniques or even the outer dielectric can be replaced by a metamaterial of permittivity lower than one (metahorns). A semispherical lens is added to the horn at the aperture. Then, we use a geometry of the horn based on the structure of the Figure 7, but with a profiled taper, smoothing the shape of the throat and a lens at the aperture. We keep the geometrical dimensions of the horn, that is, the length (without the lens), the diameter of the circular waveguide and the gap between the two layers of dielectrics (Figure 10).

In order to get a light horn, the outer material is chosen to be made of foam with a permittivity close to one; in our case, $\varepsilon'_r = 1.04$ at $f = 10$ GHz. The permittivity of the inner material can be chosen by an optimization process. The speed of the current method to analyze the horn allow us to decide the material of the dielectric core

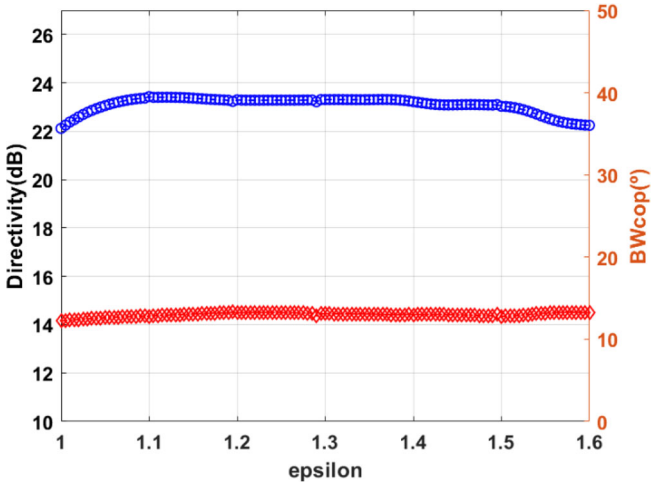

FIGURE 11 Directivity and beam-width of the horn with different materials in the core.

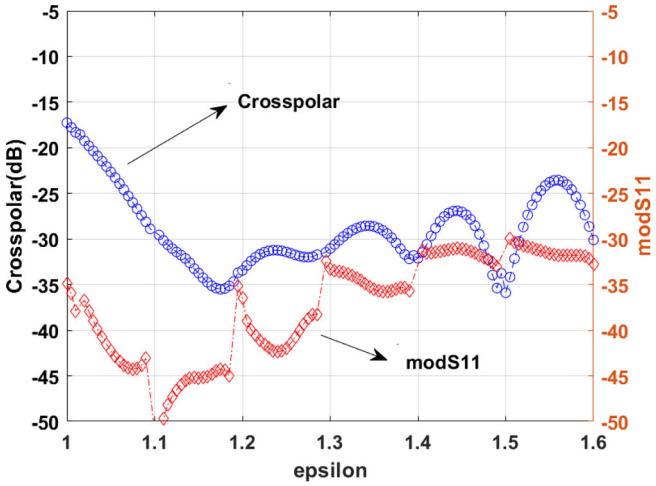

FIGURE 12 Cross-polar(dB) and module of S11 parameter (dB) of the horn with different materials in the core.

in order to achieve an optimal performance of the antenna.

After a numerical convergence study, we use a mesh with 10 063 elements of order (1, 2, 2) as explained at the beginning of the article; a sphere of radius = 11 705 cm, surrounding the antenna; a distribution of 5 modes of circular waveguide at the input port and 100 spherical modes at the port simulating the radiation. In Figure 11, we show a study of the directivity and the copolar pattern beam-width of the horn with different materials, indicating to the designer the best option to give priority to one of the radiation parameters.

In Figure 12, we show a similar study for the peak cross-polar pattern and the reflection at the throat of the antenna.

TABLE 5 Performance of the optimized horn.

D (dB)	EA (%)	XP (dB)	BWcop (°)	VSWR
23.4	84.8	−36.8	13	1.03

Abbreviations: BWcop, beam width in the copolar; EA, efficiency of aperture; VSWR, voltage standing wave ratio; XP, peak of the cross-polar.

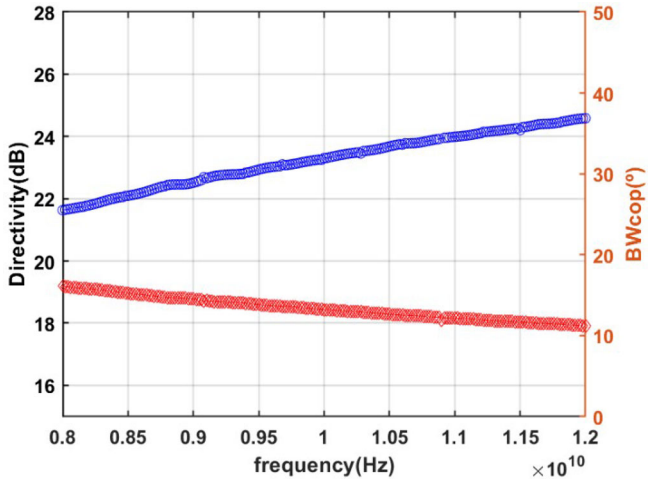

FIGURE 13 Directivity and Beam width copolar in relation to the frequency, for a profiled horn with a dielectric core and lens.

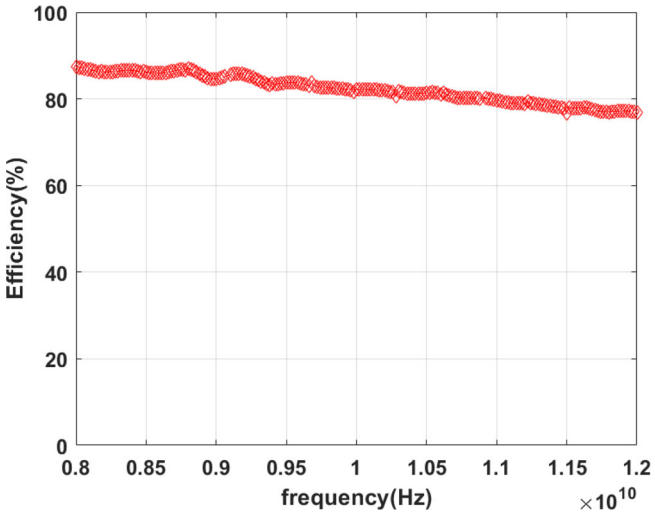

FIGURE 14 Efficiency of Aperture in relation to the frequency, for a profiled horn with a dielectric core and lens.

If we decide to use the optimal value of the permittivity ($\varepsilon_r = 1.2$), we obtain the following parameters at $f = 10$ GHz (Table 5):

We have checked that all the parameter of the antenna result improved in relation to the horn without the lens; moreover, the lens increases the length of the antenna 6.5 cm (22%). This design constitutes a good alternative to be used in this range of frequency.

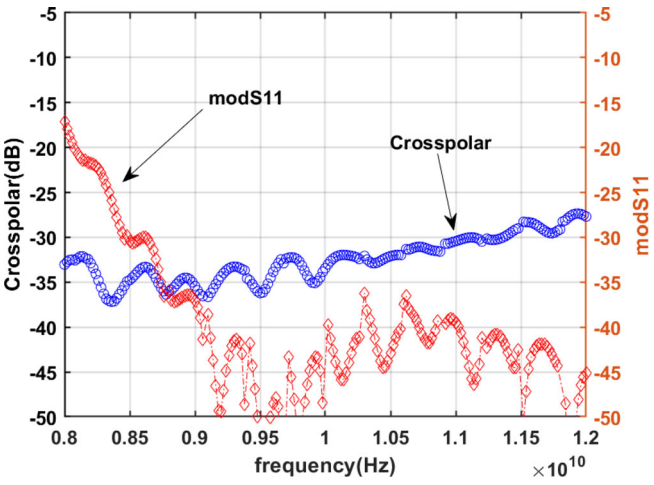

FIGURE 15 Peak cross-polar level and module of S11 in relation to the frequency, for a profiled horn with a dielectric core and lens.

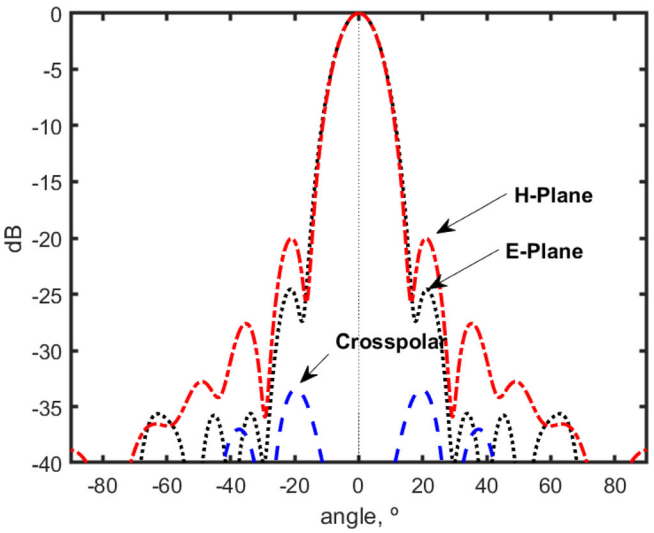

FIGURE 16 Normalized radiation pattern and peak cross-polar level, for a profiled horn with a dielectric core and lens.

Once we have achieved an optimized design of the horn, it is important to check the frequency behavior of the antenna. The behavior of the antenna versus the frequency is explored and shown in the following figures. In Figures 13–15, the directivity, the beamwidth, the efficiency, the peak cross-polar and the module of the S11

versus the frequency are shown. From these figures, we notice a good performance of the antenna along a wide band of frequencies. The oscillating behavior of the module of S11 can be due to some reflections at the aperture surface.

In Figure 16, we show the normalized radiation pattern of the horn as well as the peak cross-polar level.

4 | CONCLUSIONS

A reliable and simple method to develop higher-order curved hierarchical div-conforming hybrid elements, free of spurious modes for any order, has been presented. The vector space of functions is decomposed into three subspaces and a discussion about the combination of the different orders of the subspaces is presented in order to get families of higher-order elements avoiding the presence of spurious modes. Some applications based on BOR are presented and the robustness of the procedure is employed to achieve a deep study of conical horn antennas loaded with dielectrics and lenses.

DATA AVAILABILITY STATEMENT

The data that support the findings of this study are available from the corresponding author upon reasonable request.

ORCID

José M[a]. Gil https://orcid.org/0000-0001-7335-1483

REFERENCES

1. Hernández-Gil F, Pérez Martínez J. Analysis of dielectric resonators with tuning screw and supporting structure. *IEEE Trans Microw Theory Tech*. 1985;33:1453-1457.
2. Gil JM. CAD-oriented analysis of cylindrical and spherical dielectric resonators in cavities and MIC environments by means of finite elements. *IEEE Trans Microw Theory Tech*. 2005;53(9):2866-2874.
3. Lee JF, Wilkins GM, Mittra R. Finite-element analysis of axisymmetric cavity resonator using a hybrid edge element technique. *IEEE Trans Microw Theory Tech*. 1993;41:1981-1987.
4. Lee JF, Sun DK, Cendes ZJ. Full-wave analysis of dielectric waveguides using tangential vector finite elements. *IEEE Trans Microw Theory Tech*. 1991;39(8):1262-1271.
5. Gil JM, Monge J, Rubio J, Zapata J. A CAD-oriented method to analyse and design radiating structures based on bodies of revolution by using finite elements and generalized scattering matrix. *IEEE Trans Antennas Propag*. 2006;54:899-907.
6. Garcia-Contreras G, Córcoles J, Ruiz-Cruz JA. 2-D FEM formulation for closed waveguides with magnetically biased graphene sheets. *IEEE Trans Terahertz Sci Technol*. 2022;12(1):98-101.
7. Garcia-Contreras G, Córcoles J, Ruiz-Cruz JA. Degeneracy-discriminating modal FEM computation in higher-order rotationally symmetric waveguides. *IEEE Trans Antennas Propag*. 2021;69:8003-8008.
8. Rui X, Hu J, Liu QH. Higher-order finite element method for inhomogeneous axisymmetric resonators. *Prog Electromagn Res B*. 2010;21:189-201.
9. Gil JM, Webb JP. On the 2-D applications of high-order vector finite elements to the study of electromagnetic resonance. *IET Microw Antennas Propag*. 2007;1(2):306-313.
10. Di Wu, Zhenghe Feng I, Xiao Zhuang, "A novel focusing lens conical horn antenna loaded with dielectric, IEEE International Wireless Symposium (IWS), 2015.
11. Mustafa K, Al-Nuaimi T, Hong W, Zhang Y. Design of high-directivity compact-size conical horn lens antenna. *IEEE Antennas Wirel Propag Lett*. 2014;13:467-470.
12. Webb JP. Hierarchical vector basis functions of arbitrary order for triangular and tetrahedral finite elements. *IEEE Trans Antennas Propag*. 1999;47:1244-1253.
13. Sun DK, Cendes Z. Fast high-order FEM solutions of dielectric wave guiding structures. *IEE Proc Microw Antennas Propag*. 2003;150(4):230-236.
14. Gentili GG, Bolli P, Nesti R, Pelosi G, Toso L. High-order FEM mode matching analysis of circular horns with rotationally symmetric dielectrics. *IEEE Trans Antennas Propag*. 2007;55(10):2915-2918.
15. Guan JM, Su CC. Resonant frequencies and field distributions for the shielded uniaxially anisotropic dielectric resonator by th FD-SIC method. *IEEE Trans Microw Theory Tech*. 1997;45:1767-1777.
16. Krupka J, Derzakowski K, Abramowicz A, Tobar ME, Geyer RG. Use of whispering-gallery modes for complex permittivity determinations of ultra-low-loss dielectric materials. *IEEE Trans. Microw Theory Tech*. 1999;47:752-759.
17. Greenwood AD, Jin JM. A novel efficient algorithm for scattering from a complex BOR using mixed finite elements and cylindrical PML. *IEEE Trans Antennas Propag*. 1999;47(4):629.
18. Rubio J, Gonzalez MA, Zapata J. Analysis of cavity-backed microstrip antennas by a 3-D finite element/segmentation meted and a matrix Lanczos-Padé algorithm (SFELP). *IEEE Antennas Wirel Propag Lett*. 2002;1:193-195.
19. Olver AD, Clarricoats PJB, Kishk AA, Shafai L. *Microwave Horns and Feeds*. IEEE Press; 1994.
20. Zhang S, Cadman D, Vardaxoglou JYC. Additively manufactured profiled conical horn Antanna with dielectric loading. *IEEE Antennas Wirel Propag Lett*. 2018;17(11):2128-2132.
21. Rolland A, Ettorre M, Drissi MH, Le Coq L, Sauleau R. Optimization of reduced-size smooth-walled conical horns BoR-FDTD and genetic algorithm. *IEEE Trans Antennas Propag*. 2010;58(9):3094-3100.

How to cite this article: Gil JM. Robust numerical approximation of 2.5-dimensional electromagnetic problems by using finite elements. *Int J RF Microw Comput Aided Eng*. 2022;e23363. doi:10.1002/mmce.23363